

New Synthesis of Polycrystalline NiSe Nanoarrays on Ni Foam as the Electrode for High Performance Supercapacitors

Han Chen, Liting Wu, Kaiyou Zhang*, Aimiao Qin, Shuoping Chen

Guangxi Ministry-Province Jointly-Constructed Cultivation Base for State Key Laboratory of Processing for Non-ferrous Metal and Featured Materials, College of Materials Science and Engineering, Guilin University of Technology, Guilin 541004, P. R. China

*E-mail: kaiyou2014@glut.edu.cn

Received: 6 May 2018 / *Accepted:* 29 July 2018 / *Published:* 5 November 2018

The novel aloe leaf-like polycrystalline NiSe nanoarrays grown on the nickel foam are synthesized by one-step hydrothermal method with adding lauramidopropyl betaine (LAB) as the surfactant. The prepared NiSe nanoarrays are characterized by XRD, EDS and FE-SEM. As the electrode for the supercapacitor, the as-prepared NiSe@Ni electrode exhibits high electrochemical performance with an areal specific capacitance of 1.55 F cm^{-2} at the current density of 4 mA cm^{-2} and the capacitance retains 67% of the initial capacitance value after 1000 cycles. Moreover, the asymmetric supercapacitor (ASC) of NiSe//AC (active carbon) is also fabricated by using the NiSe nanoarrays as positive electrode and the active carbon as negative electrode and 1 M KOH solution as the electrolyte. The operating voltage of NiSe//AC ASC can be increased to 1.6 V, at the same time the ASC possesses high energy density (2.67 mWh cm^{-3} at the power density of 46.2 mW cm^{-3}) and retains 72.7 % of initial capacitance after 1600 cycles at current density of 20 mA cm^{-2} .

Keywords: NiSe; aloe leaf-like; nanoarrays; asymmetric supercapacitor

1. INTRODUCTION

Renewable energy has been increasingly utilized due to the shortage of fossil fuel, and energy storage would achieve sustainable and rapid development [1]. As an alternative device, supercapacitors (SCs), also called electrochemical capacitors, have been developing as a typical energy storage and conversion devices with high power density and long cycle-life [2]. Electrical double layer capacitors (EDLCs) and pseudocapacitors (PCs) are two categories of supercapacitors based on the different charge storage mechanism. In general, various carbon materials [3] (activated carbon, carbon nanotubes,

graphene etc.) with high specific surface and chemical stability are used as the conventional electrode materials for EDLCs. While the pseudocapacitive electrode materials mainly include the transition metal oxides (TMO) and conductive polymers with high energy density [4].

Since the discovery of the pseudocapacitance of RuO₂, the pseudocapacitance characteristics of various metal oxides (e.g. MnO₂ [5], CuO [6] and NiO [7]) have been constantly explored. Yet, most of the metal oxides showed poor electrical conductivity, such as the low intrinsic conductivity (10⁻⁶-10⁻⁵ S/cm) of MnO₂ [8]. The electrode materials played an important role in the application of supercapacitor. It is significant to synthesize electrode materials with novel nanostructures to obtain excellent conductive property by new preparation process. Generally, the active substance and the binder are mixed evenly and then pressed on the current collector [9]. However, in recent years, it has been trended to grow active materials on the current collector directly as an electrode material without binder, which would strengthen the interaction between the electrode material and the current collector, meanwhile reduce the resistance. Abhik Banerjee et al. [10] devised a method for hydrothermal synthesis of hollow Co_{0.85}Se nanowire arrays on carbon fiber paper with the impressive areal specific capacitance of 929.5 mF cm⁻² (at 1 mA cm⁻²).

Morphology is an important factor in designing new nanomaterials, and it has the functional characteristics in controlling electrochemical applications [2, 11]. Especially for the 1D nanostructure (nanorod, nanowire, nanoribbon etc.) which can provide a direct electron transport pathway and high aspect ratio to facilitate the penetration of electrolyte and maximize the utilization of active substances [12]. Lu et al. [13] fabricated NiO nanorod arrays with ultrahigh specific capacitance of 2018 F g⁻¹, which was closed to the theoretical value of 2573 F g⁻¹. Wang et al. [14] designed and synthesized CoS₂ and MoS₂/CoS₂ nanotube arrays insitu grown on Ti plate, which displayed a relatively high areal specific capacitance of 142.5 mF cm⁻² at 1 mA cm⁻².

Transition metal sulfides (TMS) have been also widely investigated as alternative electrochemical electrode materials with good electronic conductivity [15]. Chen et al. [16] had synthesized high conductive urchin-like NiCo₂S₄ nanostructures with outstanding rate capability. Selenium (Se) is a member of chalcogen, and it was reported that the metallic property of Se was more obvious than O, suggesting the better electronic property [17]. NiSe, as a typical electrode material, has excellent electrical, magnetic and catalytic properties, which has been widely used in Li-ion batteries [18], dye-sensitized solar cells [19], hydrogen evolution reactions [20] and supercapacitors [21-23], showing good potential application value. Peng et al. [23] reported novel NiSe@MoSe₂ nanosheet arrays grown on the nickel foam through a facile one-step hydrothermal method, and it exhibited a specific capacitance of 223 F g⁻¹ at a current density of 1 A g⁻¹ and a high rate performance. Guo et al. [22] used solvothermal method (N,N dimethylformamide as solvent) to synthesize the nanosheet-grading multilayer microsphere NiSe. They also explored the effect of the surfactant of CTAB on the morphology. As a kind of supercapacitor electrode materials, the specific capacitance of NiSe reached as high as 492 F/g at a constant current density of 0.5 A/g. And the asymmetric supercapacitor (ASC) of NiSe//AC (active carbon) was also assembled whose specific capacitance was 80 F/g, providing a basis for such material as supercapacitor. However, there was no report about the NiSe nanoarrays with the aloe leaf-like morphology to the best of our knowledge, especially using lauramidopropyl betaine (LAB) as the surfactant.

In this study, we synthesized one dimension nanoarrays of polycrystalline NiSe with novel aloe leaf-like morphology on the nickel foam (NiSe@Ni) by a facile one-step hydrothermal method with adding LAB as the surfactant. We found that the NiSe@Ni nanoarrays displayed a high areal specific capacitance of 1.55 F cm^{-2} at the current density of 4 mA cm^{-2} . Based on the good electrochemical performance of NiSe nanoarrays, we used the as-prepared NiSe@Ni electrode as the positive electrode and active carbon (AC) on Ni foam (AC@Ni) as the negative electrode to assemble the NiSe//AC asymmetric supercapacitor (ASC). The electrochemical performance of NiSe//AC ASC was also systematically investigated. The potential window of the NiSe//AC ASC could be extended to 1.6 V and the energy density could achieve to 2.67 mWh cm^{-3} with power density of 46.2 mW cm^{-3} .

2. EXPERIMENTAL

2.1 Materials

All the chemical reagents were of analytical grade and were used as received without further purification. The reagents used in this study included Se powder, hydrazine hydrate ($\text{N}_2\text{H}_4 \cdot \text{H}_2\text{O}$, 80%), ethanol, hydrochloric acid (HCl), lauramidopropyl betaine (LAB, 35%), toluene, acetone, activated carbon (AC), poly vinylidene fluoride (PVDF) and N-methyl pyrrolidone (NMP). The nickel foam ($1.5 \times 1.5 \times 0.1 \text{ cm}^3$) slices were cleaned with toluene, acetone, ethanol and deionized water in sequence with the KQ3200DE-type ultrasonic cleaner for three times and dried in an electric oven at 60°C for 2h, and then they were immersed in a 2.4 mol/L HCl solution for 15 min and rinsed with ethanol to remove the oxide layer on the surface of nickel foam before they were used to fabricate electrode materials.

2.2 Synthesis of aloe leaf-like polycrystalline NiSe nanoarrays

The aloe leaf-like polycrystalline NiSe nanoarrays were prepared by a facile one-step hydrothermal method with LAB as the surfactant. Typically, an amount of 0.75 mmol of Se powder was dissolved in a mixture solution of 2 mL of $\text{N}_2\text{H}_4 \cdot \text{H}_2\text{O}$ and 15 mL of deionized water at room temperature, and then 0.15g of LAB was added to the mixture under vigorously magnetic stirring. Then, a piece of pretreated nickel foam ($1.5 \times 1.5 \times 0.1 \text{ cm}^3$) was immersed in the above prepared mixed solution and transferred into a 25 mL Teflon-lined stainless-steel autoclave which was sealed and maintained at 140°C for 24 h in an oven. After it was cooled down to room temperature naturally, the sample was rinsed with deionized water and ethanol for several times and then dried at 60°C for 6 h in vacuum oven, and finally the NiSe@Ni electrode was obtained. In order to investigate the influence of LAB on the structure and morphology of NiSe@Ni, the samples with adding 0 g and 0.3 g of LAB by the same synthetic route were also prepared.

2.3 Fabrication of NiSe//AC ASC

The NiSe//AC asymmetric supercapacitor was fabricated for higher energy density and greater potential window by using the as-synthesized NiSe@Ni electrode as the positive electrode and the AC electrode as the negative electrode. The two electrodes were fabricated face to face separated by membrane and immersed into 1 M KOH electrolyte to form the NiSe//AC ASC. The mass ratio of NiSe to AC was calculated to keep a charge balance ($q^+ = q^-$). In the process of preparation of AC electrode, the activated carbon, acetylene black and PVDF binder were mixed with the weight ratio of 8:1:1 in a small amount of NMP to form homogeneous slurry, and then the slurry was drop onto the surface of nickel foam ($1 \times 1.5 \text{ cm}^2$) and dried at $110 \text{ }^\circ\text{C}$ for 12h in vacuum oven. Finally, the nickel foam coated with AC was pressed under 10 MPa for 3 min to form an AC@Ni electrode.

2.4 Characterization of electrode materials

The crystal structure of the sample was investigated by X-ray diffraction (XRD, PANalytical X'Pert) with Cu K α radiation ($\lambda = 1.5406 \text{ \AA}$). The morphology was characterized by field-emission scanning electron microscope (FE-SEM, S-4800) with an energy disperse spectroscopy (EDS, Xmax50) attachment.

2.5 Electrochemical measurements

The supercapacitor performance was investigated by cyclic voltammetry (CV), galvanostatic charge/discharge (GCD), electrochemical impedance spectroscopy (EIS) and cycling stability tests using an electrochemical workstation (CHI 690) with 1 M KOH as electrolyte. The NiSe@Ni foam electrode was investigated in a traditional three-electrode system, in which a platinum foil ($1 \times 1 \text{ cm}^2$) was used as the counter electrode, a mercuric oxide electrode (Hg/HgO) was used as the reference electrode and NiSe@Ni electrode was used as working electrode. While the NiSe//AC asymmetric supercapacitor was tested in two-electrode system with NiSe@Ni as the positive electrode and AC@Ni as the negative electrode, respectively.

It is well known that the specific capacitances of the supercapacitor can be estimated from CV and GCD curves based on the following equations [24]:

$$C_a = \frac{\int I(V) dV}{2\nu S \Delta V} \quad (1)$$

$$C_s = \frac{I \times \Delta t}{S \times \Delta V} \quad (2)$$

Where C_a and C_s (F cm^{-2}) are the areal specific capacitance, and I , Δt , ν , S and ΔV represent the discharge current (A), the discharge time (s), the scan rate (mV s^{-1}), the area of electrode (cm^2) and the voltage variation (V) during the discharge process after potential drop, respectively.

However, the energy density (E , mWh cm⁻³) and power density (P , mW cm⁻³) of ASC in unit volume can be evaluated by equation (3) and (4) [24]:

$$E = \frac{I \times \Delta t}{7200 Vol} \Delta V \quad (3)$$

$$P = \frac{3600 E}{\Delta t} \quad (4)$$

Where I , Δt , Vol and ΔV represent the discharge current (mA), the discharge time (s), the volume of ASC (cm³) and the voltage variation (V) during the discharge process after potential drop, respectively.

3. RESULTS AND DISCUSSION

3.1 Characterization of NiSe@Ni electrode

The as-synthesized NiSe@Ni electrodes were first characterized by XRD. Fig. 1(a) displayed the XRD patterns of the as-obtained samples on the nickel foam with adding 0g, 0.15g and 0.3g of LAB. The peaks obviously observed at 2θ of 44.6°, 51.9° and 76.6° in the three patterns were assigned to the base of nickel foam (JCPDS No. 70-0989). And the peaks located at 2θ of 30.9°, 33.9°, 38.5°, 46.5°, 53.6°, 55.0° and 56.1° could be assigned to makinenite NiSe (JCPDS No. 89-2058), and the corresponding crystal planes were (300), (021), (211), (131), (321), (330) and (012), respectively. The other peaks in Fig. 1(a) located at 2θ of 32.8°, 44.4°, 49.8°, 59.6°, 60.9° and 68.9° could be assigned to sederholmite NiSe (JCPDS No. 75-0610), and the corresponding crystal planes were (101), (102), (110), (103), (201) and (202), respectively. Anyway, the other small peaks could also be consistent with either makinenite NiSe or sederholmite NiSe. The XRD patterns showed that the as-prepared NiSe samples were polycrystalline structure comprising of makinenite and sederholmite NiSe phases. The EDS spectrum of NiSe@Ni was shown in Fig. 1(b), revealing the existence of the main elements of Ni and Se, however, a little oxygen signal was also detected which may be from the absorbed moisture and oxygen on the surface of the samples [10].

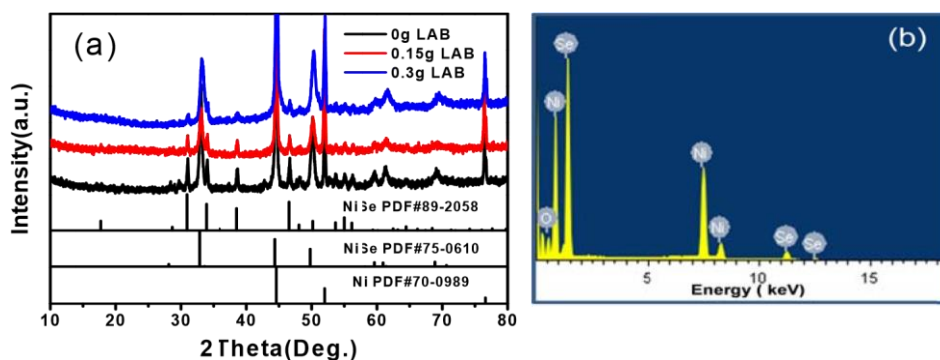


Figure 1. (a) X-ray diffraction patterns of the as-synthesized NiSe@Ni with adding different amount of LAB, (b) EDS of NiSe@Ni with adding 0.15g of LAB.

The morphology and size of the as-synthesized products were clearly characterized by FE-SEM. Fig. 2(a) showed the FE-SEM image of the cleaned Ni foam, displaying a smooth surface and clear crystal boundary, while Fig. 2(b) exhibited rough surface of Ni foam after treated with 2.4 mol/L HCl for 15 minutes. The FE-SEM images of the sample without adding LAB surfactant were shown in Fig. 2(c, d), appearing the wrinkled surface morphology. However, the morphology completely changed to novel aloe leaf-like nanoarrays after adding LAB surfactant as presented in Fig. 2(e, f, g, h) with different magnification. It can be seen that the NiSe nanoneedles grown on the surface of nickel foam display a uniform distribution in the low magnification micrograph (Fig. 2(e, g)). In addition, the high magnification micrographs (Fig. 2(f, h)) obviously exhibited the novel aloe leaf-like single nanoneedle of NiSe with the average length of about 520 nm, which revealed that the size and morphology of NiSe would be controlled during the synthesis process by adding LAB surfactant. It can be also seen that the aloe leaf-like morphology of NiSe growth on Ni foam with adding 0.15g of LAB was more obvious than that of adding 0.3g of LAB or without adding LAB, which might be due to the selective absorption of LAB surfactant on the crystallographic facets during crystal growth [25, 26], and the amount of 0.15g of LAB was the optimum dosage. Moreover, the inset in Fig. 2(f) showed the photo of real aloe, and the sample displayed the similar morphology. The aloe leaf-like nanoarrays were helpful for increasing the contact between NiSe and electrolyte. Therefore, its electrochemical properties could be improved [22].

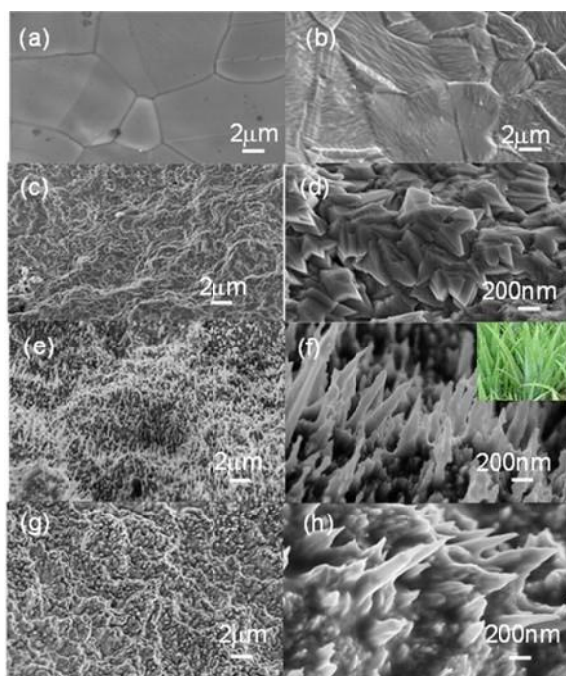


Figure 2. FE-SEM images of (a) the cleaned Ni foam, (b) Ni foam after immersed in 2.4 mol/L HCl solution, (c, d) the as-obtained sample without adding LAB, (e, f) NiSe with adding 0.15g of LAB, the inset in Fig. 2 (f) is the photo of aloe, (g, h) NiSe with adding 0.3g of LAB.

3.2 Electrochemical performance of NiSe@Ni electrode

The electrochemical properties of the as-obtained NiSe@Ni electrode were investigated by CV,

GCD and EIS techniques, using the three-electrode system in 1 M KOH electrolyte. Fig. 3(a) showed the CV curves of the as-obtained NiSe@Ni electrode with and without adding LAB at a scan rate of 10 mV s^{-1} with potential window ranging from 0 to 0.6 V. It was clear that the area of the CV curve of NiSe@Ni with adding 0.15 g of LAB was obviously larger than that of adding 0 g and 0.3 g of LAB, indicating the higher capacitance of NiSe@Ni with adding 0.15 g of LAB, which can be further proved by GCD curves. Fig. 3(b) presented the GCD curves of the as-obtained electrode with and without adding LAB at a current density of 8 mA cm^{-2} from 0 to 0.5 V, revealing that the NiSe@Ni electrode with adding 0.15 g of LAB displayed a higher areal specific capacitance (1.12 F cm^{-2}) than that of the sample with adding 0.3 g of LAB (1.05 F cm^{-2}) and without adding LAB (0.78 F cm^{-2}) according to the Eqn. (2). The results revealed that the higher capacitance of NiSe@Ni with adding 0.15 g of LAB could benefit from the aloe leaf-like nanoarrays morphology which provided larger surface area for electrochemical reaction between the electrolyte and the electrode. The resistance of the as-prepared electrodes was analyzed by EIS. Fig. 3(c) showed the Nyquist plots of the as-prepared electrodes obtained over the frequency range from 0.01 Hz to 100 kHz at the corresponding open circuit potential, with an expanded view of the high frequency region in the inset. There were two regions in the plots: a semicircle in the high frequency region and a straight line in the low frequency region, respectively. The intersection of the semicircle and the x-axis represented the series resistance (R_s) of the entire electrode, and the slope of the straight line represented the diffusion resistance (R_w) between the electrolyte and the electrode. As can be seen from Fig. 3(c), the series resistance of NiSe@Ni electrodes with adding 0 g, 0.15 g and 0.3 g of LAB were 3.37Ω , 2.77Ω and 3.04Ω , respectively. It was obvious that the series resistance of the NiSe@Ni electrode with adding 0.15 g of LAB was the smallest, which could be ascribed to the aloe leaf-like nanoarrays structure providing passages for electron transfer.

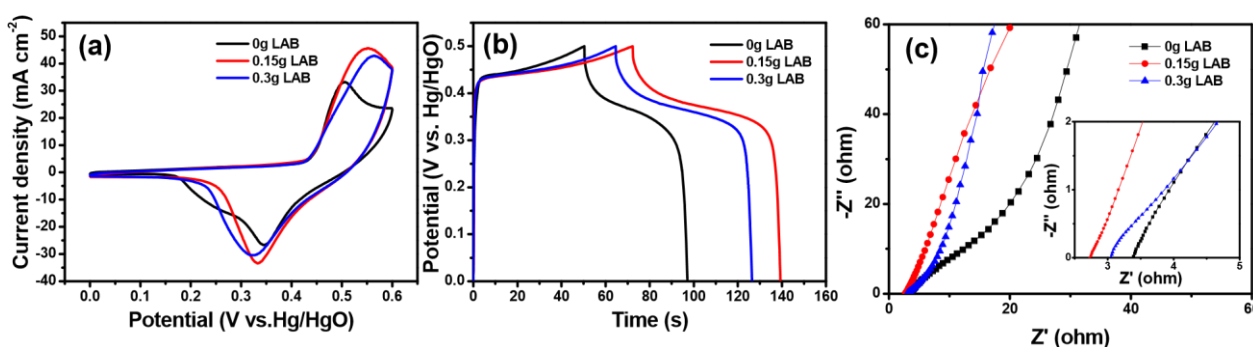


Figure 3. Electrochemical performance of NiSe@Ni electrodes with adding 0 g, 0.15 g and 0.3 g of LAB: (a) CV curves at scan rate of 10 mV s^{-1} , (b) GCD curves at the current density of 8 mA cm^{-2} , (c) Nyquist plots obtained over the frequency range from 0.01 Hz to 100 kHz at the corresponding open circuit potential

The electrochemical performance of NiSe@Ni electrode with novel aloe leaf-like nanoarrays morphology was further characterized in detail. The CV curves of the as-synthesized NiSe@Ni electrode with adding 0.15 g of LAB tested in 1 M KOH solution at different scan rates from 2 to 30 mV s^{-1} in the potential window of $0 \square 0.6 \text{ V}$ were shown in Fig. 4 (a). All CV curves of NiSe@Ni foam electrode

exhibited a pair of redox peaks, which were different from the electric double-layer capacitance, attributed to the pseudocapacitive behavior of NiSe. It can be seen that the oxidation peak locates at about 0.5 V and the reduction peak locates at about 0.34 V at the scan rate of 2 mV s⁻¹, which would be explained by the reversible redox reaction [23]:



Besides, the oxidation peaks shift to higher potential and the reduction peaks shift to lower potential with increasing the scan rates, which indicates the low resistance of the electrode and the super-fast transporting rate of electrons and ions because of the good contact between NiSe and nickel foam [27]. The areal specific capacitance (C_a) of NiSe@Ni electrode at different scan rates were calculated according to Eqn. (1), and the values were 1.73, 1.3, 1.0, 0.9 and 0.6 F cm⁻² at the scan rate of 2, 5, 10, 15 and 30 mV s⁻¹, respectively, as shown in the Fig. 4 (b). The gradual decrease of capacitance with increase of scan rate was attributed to the insufficient reaction of active material in the redox reaction at higher scan rates [28].

The GCD curves of the as-synthesized NiSe@Ni foam electrode at various current densities in the potential window of 0–0.5 V in 1 M KOH solution electrolyte were shown in Fig. 4 (c). It can be seen that there exist the platforms from 0.3 V to 0.4 V in all curves, revealing the pseudocapacitance property of the NiSe@Ni foam electrode. Furthermore, the needle aloe leaf-like morphology of NiSe would increase the active surface area for insertion and desorption of OH⁻ from electrolyte, at the same time, it would also shorten the diffusion path distance for electrons and ions [29]. The areal specific capacitances at different current densities were calculated based on Eqn. (2) and the results were shown in Fig. 4 (d). The NiSe@Ni electrode exhibited an areal specific capacitance as high as 1.55 F cm⁻² at a low current density of 4 mA cm⁻², while the value decreased to 0.87 F cm⁻² at a high current density of 12 mA cm⁻². However, the areal specific capacitance was still higher than some other similar electrode materials, such as Co_{0.85}Se nanowire arrays on carbon fiber paper (929.5 mF cm⁻² at 1 mA cm⁻²) [10], the Ni_{0.85}Se (1.34 F cm⁻² at the current density of 1 A g⁻¹ (1.2 mA cm⁻² obtained according to this reference)) [30] and the MoS₂/CoS₂ nanotube arrays insitu grown on Ti plate (142.5 mF cm⁻² at 1 mA cm⁻²) [14]. The comparison of specific capacitance between NiSe in this work and some other similar electrode materials was presented in Table 1.

Table 1. The comparison of NiSe in this work with similar electrode materials for supercapacitors

<i>Materials</i>	C_s (F cm ⁻²)	I (mA cm ⁻²)	<i>Ref.</i>
NiSe	1.55	4	This work
Co _{0.85} Se	0.93	1	[10]
Ni _{0.85} Se	1.34	1.2	[30]
MoS ₂ /CoS ₂	0.14	1	[14]
α-MnO ₂	0.15	1.6	[5]
NiO/CuO	0.56	2	[6]
Ni(OH) ₂	0.24	0.01	[9]

The Nyquist plots of the NiSe@Ni foam electrode tested before and after 1000 cycles over the frequency range from 0.01 Hz to 100 kHz were shown in Fig. 5(a). Obviously, the R_s values were almost unchanged before and after 1000 cycles. However, the slope of the straight line after 1000 cycles was decreased, indicating the presence of the greater diffusive resistance of the NiSe@Ni foam electrode after 1000 cycles. Fig. 5(b) presented the capacitance retention ratio of the NiSe@Ni electrode at a current density of 20 mA cm⁻² for 1000 cycles. It revealed that the specific capacitance of the NiSe@Ni electrode reached up to 115% during the initial 250 cycles, which was still higher than that of the reported value of NiSe (84.6% of the initial specific capacitance at the current density of 0.5A g⁻¹ after 200 cycles) [22], and it was attributed to the activation process of electrode.

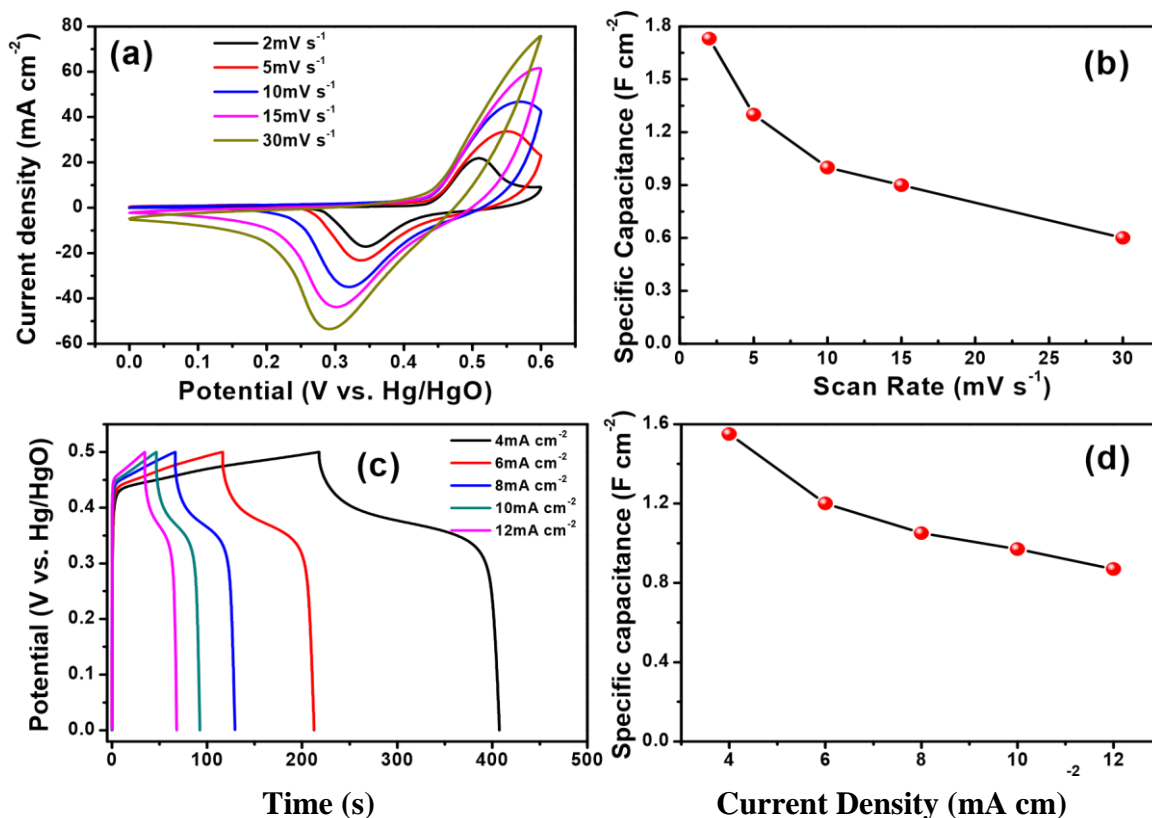


Figure 4. Electrochemical performances of the as-synthesized NiSe@Ni foam electrode with adding 0.15 g of LAB: (a) CV curves at different scan rates, (b) areal specific capacitance according to CV curves at different scan rates, (c) GCD curves at different current densities and (d) areal specific capacitance according to GCD curves at different current densities

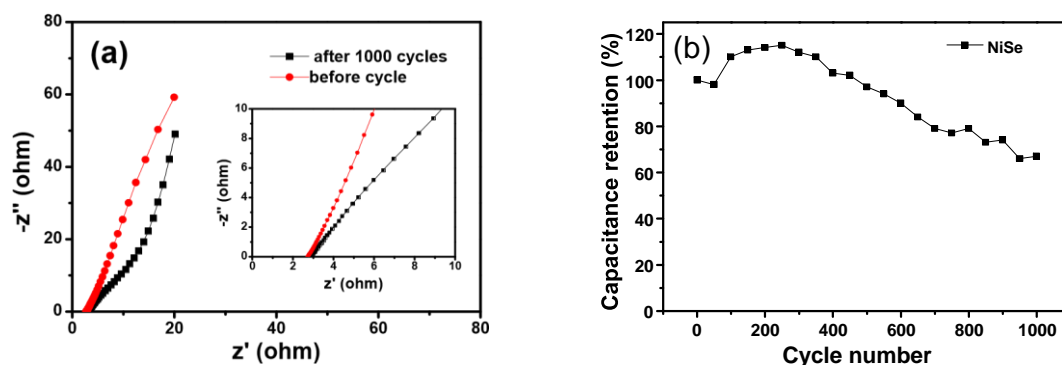


Figure 5. (a) The Nyquist plots of NiSe@Ni electrode obtained over the frequency range from 0.01 Hz to 100 kHz at open circuit potential before and after 1000 cycles, (b) capacitance retention ratio of NiSe@Ni electrode at current density of 20 mA cm⁻² for 1000 cycles.

And then the NiSe@Ni electrode retained about 67% of the initial capacitance after 1000 cycles, revealing the better stability.

3.3 Performance of NiSe//AC asymmetric supercapacitor

The electrochemical performance of the NiSe//AC ASC was measured by two-electrode system. Fig. 6(a) showed the schematic layout of NiSe//AC ASC as described in the experimental section above. The CV curves of NiSe@Ni electrode and AC@Ni electrode tested at 10 mV s⁻¹ with different potential window in three-electrode system were shown in Fig. 6(b). The rectangle shape curve (in black) of AC@Ni electrode indicated the typical double layer capacitance from the negative electrode with the potential window of -1~0 V, however, the CV curve (in red) of NiSe@Ni in Fig. 6(b) displayed a pair of redox peaks indicating the presence of faradic capacity from the positive electrode with the potential window of 0~0.6 V. According to the CV curves of NiSe@Ni and AC@Ni electrode in Fig. 6(b), we further investigate the CV curves of NiSe//AC ASC with different working potential windows from 0~0.6 V to 0~1.6 V at the scan rate of 50 mV s⁻¹, which were shown in Fig. 6(c). The shape of CV curves maintained almost similar with the potential window enlarging from 0~0.6 V to 0~1.6 V, which indicated the working potential could reach up to 1.6 V. Fig. 6(d) exhibited the CV curves of NiSe//AC asymmetric supercapacitor at various scan rates from 10 mV s⁻¹ to 100 mV s⁻¹.

It can be seen that there were no obvious oxidation-reduction peaks, which was due to the presence of the double layer capacitance of AC. And the shape of CV curves also maintained similar with the scan rate increasing. Fig. 6(e) presented the GCD curves of the NiSe//AC ASC in two-electrode system with the working potential of 0~1.6 V. The small IR drops were obtained in the discharge process, indicating the low R_s resistance of NiSe//AC ASC. Furthermore, the energy density and power density of the NiSe//AC asymmetric supercapacitor were calculated by the measured GCD curves at different current densities, as exhibited in Table 1.

Table 2. The electrochemical parameters of NiSe//AC ASC

I ($A\ cm^{-2}$)	C_s ($mF\ cm^{-2}$)	E ($mW\ h\ cm^{-3}$)	P ($mW\ cm^{-3}$)
6	810.39	2.67	46.2
8	733.16	2.35	60.8
10	656.00	2.05	75.0
12	611.35	1.86	88.8
14	560.96	1.66	102.2

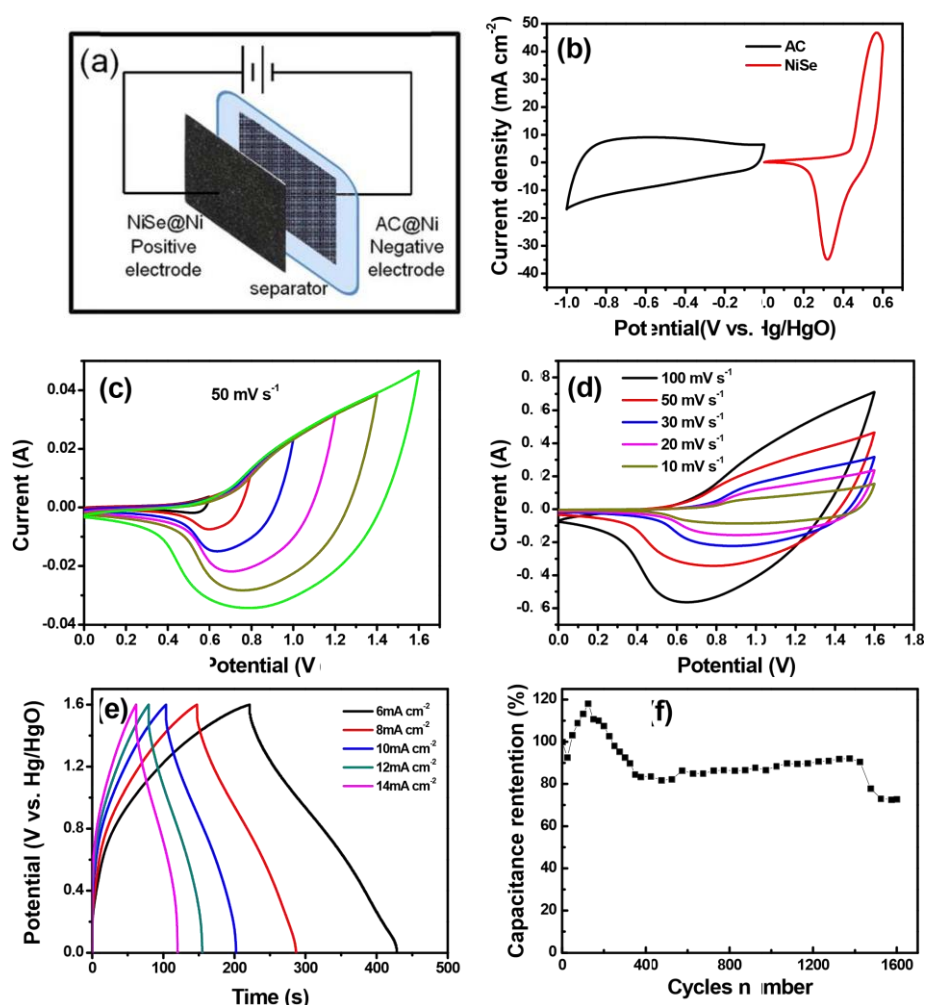


Figure 6. (a) Schematic illustration of the NiSe//AC ASC, (b) the comparison of CV curves of the NiSe@Ni and AC@Ni electrode tested in three-electrode at the scan rate of $10\ mV\ s^{-1}$, (c-d) electrochemical performances of the NiSe//AC ASC: (c) CV curves with different potential windows from 0~0.6 V to 0~1.6 V at the scan rate of $50\ mV\ s^{-1}$, (d) CV curves at different scan rates with potential window of 0~1.6 V, (e) GCD curves at different current densities, (f) cycling performance during 1600 cycles at current density of $20\ mA\ cm^{-2}$.

The results indicated that the maximum energy density obtained by our device was 2.67 mWh cm⁻³ at the power density of 46.2 mW cm⁻³, which was higher than that of the Cu_xS/CF-3h//AC (0.53 mWh cm⁻³ at power density of 4 mW cm⁻³) [31]. Fig. 6(f) showed the cycling performance of the NiSe//AC ASC recorded over 1600 cycles using GCD analysis with a current density of 20 mA cm⁻². It was observed that the specific capacitance increases to 118 % during the initial 125 cycles due to the above-mentioned activating process of the positive electrode (NiSe@Ni). And the ASC retained about 72.7 % of the initial capacitance after 1600 cycles, which was higher than the single NiSe@Ni electrode, attributing to the integrated stability performance of both the negative electrode and positive electrode.

4. CONCLUSIONS

In summary, the novel aloe leaf-like polycrystalline NiSe nanoarrays on Ni foam were synthesized by facile one-step hydrothermal method with adding LAB surfactant at 140 °C for 24h. As the electrode material for supercapacitor, the NiSe@Ni exhibited a high areal specific capacitance of 1.55 F cm⁻² at current density of 4 mA cm⁻², and the capacitance retained 67% of the initial capacitance after 1000 cycles. Furthermore, the NiSe//AC ASC was assembled in 1 M KOH electrolyte using the as-synthesized NiSe@Ni as the positive electrode and AC@Ni as negative electrode. The working voltage of NiSe//AC ASC could reach up to 1.6 V, and it possessed the energy density as high as 2.67 mWh cm⁻³ at power density of 46.2 mW cm⁻³, and it still retained 72.7% of the initial capacitance after 1600 cycles at 20 mA cm⁻². The results indicated that the NiSe@Ni could be used as a potential supercapacitor electrode.

ACKNOWLEDGEMENTS

This research was supported by Guangxi Natural Science Foundation (2016GXNSFBA380190, 2018GXNSFAA138041), Open Project Fund of Guangxi Ministry-Province Jointly-Constructed Cultivation Base for State Key Laboratory of Processing for Non-ferrous Metal and Featured Materials (14KF-10), the Doctoral Scientific Research Project of Guilin University of Technology and Guangxi Key Laboratory in Universities of Clean Metallurgy and Comprehensive Utilization for Non-ferrous Metals Resources.

References

1. P. Simon, Y. Gogotsi, *Accounts Chem. Res.*, 46 (2013) 1094-1103.
2. A.S. Aricò, P. Bruce, B. Scrosati, J.M. Tarascon, S.W. Van, *Nat. Mater.*, 4 (2005) 366-377..
3. Y.G. Wang, Y.F. Song, Y.Y. Xia, *Chem. Soc. Rev.*, 45 (2016) 5925-5950.
4. G. Wang, L. Zhang, J. Zhang, *Chem. Soc. Rev.*, 41 (2012) 797-828.
5. X. Su, X. Yang, L. Yu, G. Cheng, H. Zhang, T. Lin, F.-H. Zhao, *CrystEngComm*, 17 (2015) 5970-5977.
6. M. Huang, F. Li, Y.X. Zhang, B. Li, X. Gao, *Ceram. Int.*, 40 (2014) 5533-5538.
7. V. Kannan, A.I. Inamdar, S.M. Pawar, H.S. Kim, H.C. Park, H. Kim, H. Im, Y.S. Chae, *ACS Appl. Mater. Inter.*, 8 (2016) 17220-17225.

8. W. Guo, L. Hou, B. Hou, Y. Guo, *J. Alloy. Compd.*, 708 (2017) 524-530.
9. X. Xiong, D. Ding, D. Chen, G. Waller, Y. Bu, Z. Wang, M. Liu, *Nano Energy.*, 11 (2015) 154-161.
10. A. Banerjee, S. Bhatnagar, K.K. Upadhyay, P. Yadav, S. Ogale, *ACS Appl. Mater. Inter.*, 6 (2014) 18844-18852.
11. S.K. Shinde, G.S. Ghodake, D.P. Dubal, R.V. Patel, R.G. Saratale, D.Y. Kim, N.C. Maile, R.R. Koli, H.D. Dhaygude, V.J. Fulari, *J. Taiwan Inst. Chem. E.*, 75 (2017) 271-279.
12. Q. Yang, Z. Lu, J. Liu, X. Lei, Z. Chang, L. Luo, X. Sun, *Prog. Nat. Sci-Mater.*, 23 (2013) 351-366.
13. Z. Lu, Z. Chang, J. Liu, X. Sun, *Nano Res.*, 4 (2011) 658-665.
14. L. Wang, X. Zhang, Y. Ma, M. Yang and Y. Qi, *J. Phys. Chem. C*, 121 (2017) 9089-9095.
15. M.S. Javed, S. Dai, M. Wang, Y. Xi, Q. Lang, D. Guo, C. Hu, *Nanoscale*, 7 (2015) 13610-13618.
16. H.C. Chen, J.J. Jiang, L. Zhang, H.Z. Wan, T. Qi, D.D. Xia, *Nanoscale*, 5 (2013) 8879-8883.
17. L. Mi, H. Sun, Q. Ding, W. Chen, C. Liu, H. Hou, Z. Zheng, C. Shen, *Int. J. Hydrogen Energ.*, 41 *Int. J. Electrochem. Sci.*, Vol. 13, 2018 12595-12600.
18. Z. Zhang, X. Shi, X. Yang, *Electrochimica Acta.*, 208 (2016) 238-243.
19. C. Bao, F. Li, J Wang, P Sun, N. Huang, Y. Sun, L. Fang, L. Wang, X Sun, *Acs Appl. Mater. Interfaces*, 8 (2016) 32788-32796.
20. M.R. Gao, Z.Y. Lin, T.T. Zhuang, J. Jiang, Y.F. Xu, Y.R. Zheng, S.H. Yu, *J. Mater. Chem.J*, 22 (2012) 13662-13668.
21. B. Ye, M. Huang, Q. Bao, S. Jiang, J Ge, H. Zhao, L.Q. Fan, J.M. Lin, J.H. Wu, *Chemelectrochem*, 5 (2018) 507-514.
22. K. Guo, F. Yang, S. Cui, W. Chen, L. Mi, *Rsc Advances*, 6 (2016) 46523-46530.
23. H. Peng, J. Zhou, K. Sun, G. Ma, Z Zhang, E. Feng, Z Lei, *ACS Sustainable. Chem. Eng.*, 5 (2017) 5951-5963.
24. D. He, G. Wang, G. Liu, J. Bai, H. Suo, C. Zhao, *J. Alloy. Compd.*, 699 (2016) 706-712.
25. M.C. L'opez, G.F. Ortiz, P. Lavela, R. Alc'antara, J.L. Tirado, *ACS Sustainable Chem. Eng.*, 1 (2013) 46-56.
26. L.P. Zhu, W.D. Zhang, H.M. Xiao, Y. Yang, S.Y. Fu, *J. Phys. Chem. C*, 112 (2008) 10073-10078.
27. Y. Zhang, B. Wang, F. Liu, J. Cheng, X.-W. Zhang, L. Zhang, *Nano Energy*, 27 (2016) 627-637.
28. P. Asen, S. Shahrokhian, *J. Phys. Chem. C.*, 121 (2017) 6508-6519.
29. P. Hao, J. Tian, Y. Sang, C.C. Tuan, G. Cui, X. Shi, C.P. Wong, B. Tang, H. Liu, *Nanoscale*, 8 (2016) 16292-16301.
30. C. Gong, M.L. Huang, J.F. Zhang, M. Lai, L.Q. Fan, J.M. Lin, J.H. Wu, *Rsc Adv.*, 5 (2015) 8147481481.
31. P. Xu, C. Miao, K. Cheng, K. Ye, J. Yin, D. Cao, Z. Pan, G. Wang, X. Zhang, *Electrochim. Acta*, 214 (2016) 276-285.